^<13>N-ammonia PET-derived right ventricular longitudinal strain and myocardial flow reserve in right coronary artery disease

Kawakubo, Masateru
Department of Health Sciences, Faculty of Medical Sciences, Kyushu University

Nagao, Michinobu
Department of Diagnostic Imaging & Nuclear Medicine, Tokyo Women's Medical University

Yamamoto, Atsushi
Department of Diagnostic Imaging & Nuclear Medicine, Tokyo Women's Medical University

Nakao, Risako
Department of Cardiology, Tokyo Women's Medical University

他

出版情報：European journal of nuclear medicine and molecular imaging, 2021-12-13. European Association of Nuclear Medicine
バージョン：
権利関係：

^{13}N-ammonia PET-derived right ventricular longitudinal strain and myocardial flow reserve in right coronary artery disease

Masateru Kawakubo[a], Michinobu Nagao[b,*], Atsushi Yamamoto[b], Risako Nakao[c], Yuka Matsuo[b], Koichiro Kaneko[b], Eri Watanabe[c], Akiko Sakai[c], Masayuki Sasaki[a], and Shuji Sakai[b]

a. Department of Health Sciences, Faculty of Medical Sciences, Kyushu University, Fukuoka, Japan

b. Department of Diagnostic Imaging & Nuclear Medicine, Tokyo Women's Medical University, Tokyo, Japan

c. Department of Cardiology, Tokyo Women's Medical University, Tokyo, Japan

Authors' ORCID numbers:

Masateru Kawakubo: 0000-0003-1867-1745

Michinobu Nagao: 0000-0001-6049-8857

***Corresponding author**: Michinobu Nagao, MD

Associate Professor

Department of Diagnostic Imaging & Nuclear Medicine, Tokyo Women's Medical University

8-1 Kawada-cho, Shinjuku-ku, Tokyo 162-8666, Japan

Tel: +81-3-3353-8111

Fax: +81-3-5269-9247

E-mail: nagao.michinobu@twmu.ac.jp

Acknowledgments

This work was supported by JSPS KAKENHI Grant Number JP20K16729. We thank Editage (www.editage.com) for English language editing.

Authors' contributions

Guarantors of integrity of entire study, M.K., M.N.; study concepts/study design or data acquisition or data analysis/interpretation, all authors; manuscript drafting or manuscript revision for important intellectual

content, all authors; approval of final version of submitted manuscript, all authors; agrees to ensure any questions related to the work are appropriately resolved, all authors; literature research, M.K., M.N., A.Y; clinical studies, A.Y., R.N., Y.M.; statistical analysis, M.K., A.Y.; and manuscript editing, M.K., M.N.

Abstract

Purpose: We developed a feature-tracking algorithm for use with electrocardiography-gated high-resolution ^{13}N-ammonia positron emission tomography (PET) imaging, and we hypothesized it could be used to clarify the association between right ventricular (RV) longitudinal strain (LS) and right coronary artery (RCA) ischemia. The aim of this study was to investigate the association between the reduction of regional myocardial flow reserve (MFR) in RCA territories and PET-derived LS of the RV free wall.

Methods: Ninety-three patients with coronary artery stenosis > 50%, diagnosed by coronary computed tomography angiography, and 10 controls were retrospectively analyzed. RV-LS in the free wall was measured by a feature-tracking technique on the resting and stressed ^{13}N-ammonia PET images of horizontal long-axis slices. The patients were sub-grouped according to regional MFR values at the territories of RCA, left anterior descending artery (LAD), and left circumflex coronary artery (LCx): RCA-MFR<2.0 [n=34], RCA-MFR≥2.0 but MFR<2.0 at LAD or LCx territories [n=11], and MFR≥2.0 for all territories [n=48]. Stress and resting RV-LS were compared in each of the four groups. Multiple comparisons of RV-LS among the four groups were performed in the stress and resting state.

Results: Decreased stress RV-LS in patients with an RCA-MFR<2.0 was observed. In the patients with MFR≥2.0 for all territories, the stressed RV-LS was significantly increased compared to that in the resting state. Significantly decreased RV free-wall LS during adenosine stress in patients with RCA-MFR<2.0 was observed in the other three groups.

Conclusions: We measured RV myocardial LS using feature tracking in cine imaging of ^{13}N-ammonia PET. The results of this study suggest that PET-derived stressed RV-LS is useful for detecting reduced RV myocardial motion due to ischemia in the RCA territory.

Keywords

^{13}N-ammonia PET, right ventricular strain, high-resolution cine imaging, feature-tracking, myocardial flow reserve

Introduction

Time-of-flight systems have improved the temporal and spatial resolution of electrocardiography-gated ^{13}N-ammonia positron emission tomography (PET). This technical innovation has achieved a cinematic visualization of myocardial motion through an entire cardiac cycle. Recently, we developed an original post-processing algorithm for analyzing myocardial strains with PET imaging by applying the feature-tracking technique of cardiovascular magnetic resonance imaging [*1*]. Our technique revealed that ischemia of the coronary arteries is associated with hypokinesia in the left ventricular (LV) myocardium of the corresponding coronary artery. Furthermore, increased LV strain in non-ischemic myocardium was also revealed under adenosine stress against the resting state. In addition, myocardial flow reserve (MFR) derived from ^{13}N-ammonia PET constitutes the stress to resting ratio of myocardial blood flows and represents the relative reserve of the coronary circulation [*2-6*]. The MFR can be modeled as the 17 segments of the LV myocardium and can be displayed as a color map to obtain the regional MFR for each coronary artery territory as the right coronary artery (RCA), left anterior descending artery (LAD), and left circumflex coronary artery (LCx). Hence, PET-derived global and regional MFR are essential for the quantitative assessment of patients with myocardial ischemia. Although the association between coronary ischemia and decreased LV myocardial strain was revealed, the RCA also nourishes the right ventricular (RV) myocardium [*7*]. Longitudinal strain (LS) is a sensitive biomarker for the left and right ventricles to assess myocardial damage due to ischemia [*8-12*]. However, to the best of our knowledge, the association between MFR and RV myocardial strain, which are PET-derived parameters, has never been reported. This is because it has been difficult to image RV motion for conventional nuclear medicine due to the lack of detection of the small amount of radioisotope accumulated in the RV myocardium. Therefore, we hypothesized that the association between RV-LS and RCA ischemia could be clarified using electrocardiography-gated high-resolution ^{13}N-ammonia PET imaging. In the present study, we analyzed the association between PET-derived regional MFR and LS of the RV free wall and LV inferior wall as the RCA territory.

Materials and Methods

Study population

As part of a previous study (January 2017 to January 2019), 263 patients underwent resting/stressed myocardial ^{13}N-ammonia PET due to known or suspected coronary artery disease [*13*]. In this study, we

enrolled patients with coronary artery stenosis > 50%, diagnosed by coronary computed tomography angiography, from this cohort. All patients were over the age of 18 years and in a clinically stable state. Patients with congenital heart disease, heart failure, or a transplanted heart were excluded. In addition, we excluded two cases in which the right ventricle was not well within the PET scan area. Consequently, 93 patients were retrospectively evaluated. In addition, 10 patients with no coronary stenosis and/or a history of myocardial infarction were randomly selected from the excluded patients as controls. This study was approved by the appropriate institutional review board, and the requirement for written informed consent was waived. None of the patients had cardiovascular risk factors that were retrieved from the patients' medical records at the time of ^{13}N-ammonia PET.

^{13}N-ammonia PET scan

After the necessary preparations, the patients were positioned in a three-dimensional PET system (Biograph mCT; Siemens Healthcare, Erlangen, Germany). Repeatedly upgraded Syngo VA30A_HF07 software was used for dose correction (i.e., the difference in residual ^{13}N-ammonia activity between resting and stressed images). Sequential computed tomography scans (120 kV, 20 mA, and 3-mm slice collimation) were acquired for attenuation correction. Electrocardiogram-gated image acquisition was performed immediately after intravenous administration of ^{13}N-ammonia (approximately 185 MBq, 5 mCi), for 10 min at 16 frames/cardiac cycle using the parallel list mode [*14*]. After PET myocardial perfusion imaging was performed at rest, the adenosine stress test was performed (0.12 mg/kg/min for 6 min). Three minutes after vasodilator administration, ^{13}N-ammonia was infused (approximately 555 MBq, 15 mCi), and myocardial perfusion imaging was performed.

Assessment of myocardial blood flow via MFR

Images were reconstructed using Fourier re-binning and filtered back-projection with a 12-mm three-dimensional Hann window for the ramp filter. The reconstructed images were automatically re-orientated to the 16 short-axis, eight vertical long-axis, and eight horizontal long-axis cine images. The pixel size of the cine images was 3.2×3.2 mm, with a 3.0-mm slice thickness. Extraction of mean myocardial and cavity time-activity curves, and generation of polar maps for absolute myocardial blood flow and MFR were performed using dedicated software (Syngo MI Cardiology; Siemens Healthcare, Erlangen, Germany). Myocardial blood flow was determined based on the LV input time-activity curve and myocardial uptake using a three-compartment model and a dataset of list mode images that were obtained during the first 2 min of imaging of

the list mode data. The regional MFR values based on a 17-segment model of the RCA, LAD, and LCx territories were determined from the polar maps as the ratio of the hyperemic myocardial blood flow to the resting regional myocardial blood flow [*15*]. Global MFR was considered the mean value of the regional MFRs of the RCA, LAD, and LCx territories. Global and regional MFR values <2.0 were considered abnormal [*2*].

Longitudinal strain measurements with feature-tracking

The regional strain values of the RV free wall and LV inferior wall were semi-automatically calculated using feature-tracking analysis [*1*]. Images for strain analysis of the RV free wall and LV inferior wall were utilized in the middle slice of the heart of the horizontal long-axis and vertical long-axis, respectively. All image processing algorithms for stressed and resting PET were implemented using MATLAB R2020a (version 9.8; Mathworks Inc., Natick, MA, USA). All PET images are displayed in gray color (gamma = 1.3) with a standardized uptake value of 10–100%. First, the regional endocardial border of the ventricular wall was manually defined as a freehand line at end-diastole on the cine image. The endocardial line was replaced as the 7 points with evenly spaced points based on the line length. Second, the points were automatically tracked during a cardiac cycle using a local template-matching technique based on normalized correlation coefficient values. The initial size of the template image was set to 24×24 pixels, and the search area was set to 32×32 pixels. Finally, the ventricular regions were automatically segmented as lines with spline interpolation of the points tracked over a cardiac cycle. Systolic LSs of the RV free wall and LV inferior wall were calculated from the ventricular wall lengths using the following formula:

$$Systolic\ LS\ [\%] = \frac{Systolic\ length - Diastolic\ length}{Diastolic\ length} \times 100$$

LS takes a large negative value when the myocardium moves significantly and increases when myocardial motility decreases and approaches zero. Figure 1 shows the measurements of LS on cine PET images with points tracked by feature tracking.

Statistical analysis

All statistical analyses were performed using GraphPad Prism (version 8.1.2 Mac, GraphPad Software, La Jolla, CA). Differences were considered statistically significant at P <0.05. The Shapiro-Wilk test was used to evaluate the normality of the data distribution, and the mean and standard deviations were calculated. The stressed and resting strain values among patient groups with RCA-MFR>2.0, RCA-MFR≤2.0, LAD-

MFR<2.0, or LCx-MFR<2.0, 3 vessels MFR≥2.0, and control were multiply compared. For comparison, one-way analysis of variance or the Kruskal-Wallis test was used depending on the distribution of the data. The stress and resting LS values of each group were compared. For paired comparison, paired t-test or Wilcoxon matched-pairs signed rank test was used depending on the distribution of the data. The stressed and resting RV-LS values among the patient groups with LV inferior ischemia (RCA ischemia), without RCA ischemia but with LV ischemia (LAD/LCx ischemia), without ischemia (non-ischemia), and control were multiply compared. The presence of LV ischemia was diagnosed according to the mismatch of isotope accumulation at stress and rest states. For comparison, one-way analysis of variance or the Kruskal-Wallis test was used depending on the data distribution. The stress and resting RV-LS values of each group were compared. For paired comparison, paired t-test or Wilcoxon matched-pairs signed rank test was used depending on the data distribution. Pearson's correlation coefficients (r) or Spearman's correlation coefficients (r_S) of RV free-wall LS against the RCA-MFR, LAD-MFR, and LCx-MFR were calculated for linearly and non-linearly distributed data, respectively. Similarly, correlation coefficients of LV inferior-wall LS and regional MFRs were calculated.

Intra-observer and inter-observer reproducibility

All longitudinal strain measurements were tested for intra-observer reproducibility at 16 frames per cardiac cycle. A single observer performed all stressed and resting analyses for 30 randomly selected patients and then blindly repeated the analyses at least 1 month later. Inter-observer reproducibility was evaluated based on stressed and resting measurements for the same 30 patients, which were performed by a second observer who was blinded to the clinical and experimental data. The intra-observer and inter-observer reproducibility of the strain measurements was evaluated using Bland-Altman analyses and the intraclass correlation coefficient (ICC) with one-way random or two-way random single measures (ICC [1,1] or ICC [2,1], respectively). The ICC values were defined as excellent (≥0.75), good (0.60–0.74), moderate (0.40–0.59), or poor (≤0.39).

Results

Table 1 shows the baseline characteristics and ^{13}N-ammonia PET measurements. The number of patients with RCA-MFR<2.0, with RCA-MFR≥2.0 but MFR<2.0 at LAD or LCx territories, and with MFR≥2.0 for all territories were 34, 11, and 48, respectively. Abnormal regional MFRs were observed in the RCA (32/93 patients, 34%), LAD (33/93 patients, 35%), and LCx (34/93 patients, 37%) groups. Thirteen patients were

diagnosed with RCA stenosis ≥90% by invasive coronary angiography. Of the patients with RCA-MFR<2.0, 3 out of 8 had a history of myocardial infarction in the RCA territory. Ammonia PET showed permanent hypo-accumulation in the inferior wall in all the three patients, two of whom were considered to have non-transmural infarcts with a %uptake of approximately 50%. The other had a basal inferior wall %uptake of around 25%, which is considered a transmural infarction.

Figure 2a shows the comparison of RV-LS among the four groups at stress and resting states. Significantly decreased RV free-wall LS during adenosine stress in patients with RCA-MFR<2.0, was observed in the other three groups. There were no significant differences in the resting RV-LS among the four groups. Decreased stress RV-LS was observed against the resting state in patients with RCA-MFR<2.0. In the patients with regional MFR≥2.0 for all territories, the stressed RV-LS was significantly increased compared to that in the resting state. Figure 4 shows representative cases of RV-LS changes between the stress and resting states. A decrease in RV-LS in patients with RCA-MFR<2.0 and an increase in RV-LS in patients with regional MFR≥2.0 for all territories were observed. Figure 2b shows the comparison of LV-LS among the four groups at stress and resting states. Significantly decreased LV inferior-wall LS during adenosine stress in the three patient groups compared to the control group were observed. The resting LV-LS in the RCA-MFR<2.0 group was lower than that of the control. An increase in stress LV-LS against the resting state in the control group was observed. Figure 3 shows that the absolute value of stressed RV-LS was significantly higher than those at resting state in the non-ischemic and control groups. On the other hand, in the group with ischemia in the LV, there was no significant difference between stress and resting RV-LS. The stressed RV-LS in patients with ischemia at the LV inferior wall (with RCA ischemia) was absolutely decreased than that of the control group. Scatter plots of regional MFR and RV-LS at stress and resting states are shown in Figure 5. There were moderate correlations between stressed RV-LS and regional MFRs in each coronary territory, but there were no correlations between resting RV-LS and regional MFRs. There were no correlations between LV-LS in both stress and resting states and regional MFRs (Figure 6).

The intra- and inter-observer reproducibility for stress and resting RV free-wall LS and LV inferior-wall LS measurements are reported in Table 2. Both intra- and inter-observer reproducibility was excellent (all ICCs >0.75, $P < 0.01$), with negligible bias identified on the Bland-Altman analysis and narrow standard deviation in measurement and a narrow limit of agreement.

Discussion

There are two findings from the present study. One is that the PET-derived stressed LS in the RV free wall is associated with reduced RCA-MFR. Second, semi-automatic LS measurements via feature tracking in ^{13}N-ammonia PET imaging are simple to acquire and highly reproducible.

RV-LS in the patients with regional MFR<2.0 decreased in the stress state. This decrease was similar to the changes in the kinetics of the ischemic myocardium of the LV under adenosine stress [*16-18*]. Therefore, the reduced RV-LS was affected by RCA ischemia. Moreover, the RV-LS in the regional MFR≥2.0, non-ischemia, and control groups increased in the stress state, and these results were consistent with the changes in kinetics in adenosine-stressed normal myocardium. Comparing the RV-LS at stress and resting states among the four groups, stressed RV-LS from the RCA-MFR<2.0 and RCA ischemia groups were reduced compared to those from other groups. In the correlation analysis, stressed RV-LS was correlated to the regional MFR of the three coronary arteries, and the correlation coefficient with RCA-MFR was the highest. Consequently, it can be concluded that RV-LS has a significant association with RV-MFR, which reflects RCA ischemia under adenosine stress. In the comparison of LV-LS of the inferior wall, increased stressed LV-LS in controls, and reduced stressed LV-LS in controls compared to the other three groups were observed. In the comparison of LV-LS of the inferior wall, stressed LV-LS in controls was higher than that in resting state, and stressed LV-LS in controls was greater than in the other three groups. There were no significant correlations between LV-LS and regional MFRs. We considered two reasons why RV-LS was observed to be associated more with RCA-MFR than LV-LS. First, the contribution of the longitudinal direction for myocardial contraction was greater in the RV than in the LV. In the LV myocardium, contractions of endocardial, middle, and epicardial layers produce the long axis and short axis motions, as well as a twisting motion corresponding to systemic circulation [*19-22*]. On the other hand, in the RV myocardium, two thin myocardial layers are responsible for pulmonary circulation, mainly long-axis contraction [*23, 24*]. Second, because the LV myocardium receives blood supply not only from the RCA but also from the LAD and LCx, LV-LS did not reflect the effects of reduced RCA-MFR as strictly as RV-LS. MFR is defined as MBF under adenosine stress divided by the rest MBF. MFR is highly dependent on resting MBF, and MFR of each territory is calculated from the same dynamic data immediately after ammonia injection. Therefore, MFRs of the main coronary territories interfere with each other and are averaged out. For this reason, Kawaguchi et al. proposed relative MFR, which emphasizes abnormalities in local MFR [*25*]. RV-LS takes a negative value because the RV

length reduces during RV contraction. In other words, a low strain value is large in absolute value, which means good wall motion. The inverse correlation between RV-LS and LAD-MFR or LCx-MFR means that reduced RV wall motion is associated with reduced LV-MFR. We postulate that one reason for this correlation is that LAD-MFR or LCx-MFR decreases in parallel to the decrease in RCA-MFR. Finally, RV-LS reduction is associated with decreased LV-MFR outside the inferior wall. Based on the above, RV-LS is considered to reflect changes in myocardial motility due to RCA ischemia more strongly than LV-LS, and PET-derived RV-LS can be expected as a new clinical evaluation index for RCA ischemia. In addition, in three patients with a history of RCA infarction, the absolute mean value of the stressed RV-LS tended degraded against resting state (stress: 15.9 %, resting: 17.3 %). The residual ischemic area in the peri-infarction may have been reflected as a slight loss of wall motion during adenosine stress. To advance the clinical application of PET-derived RV-LS, we believe that further research on patients with a history of infarction is necessary.

Our feature-tracking-based semi-automatic LS measurement indicated excellent inter -and intra-observer reproducibility. Excellent reproducibility of LV-LS with PET imaging has been reported [*1*]. Compared to this previous report, the reproducibility of the RV-LS measurement using PET images is excellent. Because the RV myocardium is thin, wall motion analysis is difficult. However, feature tracking could be fully applied to high-resolution PET imaging without manual correction for the mistracking of myocardial features in this study. Furthermore, feature tracking involves a simple-to-use algorithm, and our proposed strain analysis method can automatically calculate the strain for a cardiac cycle using only manual delineation of the regional myocardial wall. Because feature tracking involves a traditional template-matching technique, the offline tool we used provides regional myocardial strain values within 10 s, which includes the time taken to manually draw the endocardial borders. In recent years, cardiovascular magnetic resonance-derived RV strain has been attracting attention as a useful clinical value for patients with pulmonary hypertension, such as pulmonary embolism or congenital heart disease [*26, 27*]. One of the great advantages of PET imaging over cardiovascular magnetic resonance is that the images at stress and resting states can be obtained in a single examination. Moreover, this analysis can be performed as needed, even after the PET examination, via post-processing strain measurements, and does not require additional image acquisition or additional radioisotope use, which enhances its potential clinical value. Therefore, our proposed PET-derived RV-LS analysis may provide novel clinical findings for various diseases in patients with pulmonary hypertension.

This study had some limitations. We analyzed a small number of patients from a single center. This limitation might be restricted by only a few cyclotrons in our country, which are required for ^{13}N-ammonia production. Nevertheless, our preliminary results suggest a significant association between PET-derived RV-LS and RCA-MFR and clinical potential for patients with RCA ischemia. Therefore, further prospective studies are needed to accumulate further evidence.

Conclusion

In conclusion, we measured RV myocardial LS using feature tracking in high-resolution cine imaging of ^{13}N-ammonia PET. The results of this study suggest that PET-derived stressed RV-LS is useful for detecting reduced RV myocardial motion due to ischemia in the RCA territory and provides reproducible quantitative values of RV motion.

STATEMENTS AND DECLARATIONS

Competing interest: There are no conflicts of interest to declare.

Funding: This work was supported by JSPS KAKENHI Grant Number JP20K16729.

Data availability: All data generated or analyzed during this study are included in this published article.

Code availability: Not applicable.

Ethics approval: This study was approved by the appropriate institutional review board.

Consent to participate: The requirement for written informed consent was waived.

Consent to publish: Not applicable.

References

1. Kawakubo M, Nagao M, Yamamoto A, Nakao R, Matsuo Y, Fukushima K, et al. ^{13}N-ammonia positron emission tomography-derived endocardial strain for the assessment of ischemia using feature-tracking in high-resolution cine imaging. J Nucl Cardiol. 2021 [Epub ahead of print] https://doi.org/10.1007/s12350-021-02677-9.
2. Fiechter M, Ghadri JR, Gebhard C, Fuchs TA, Pazhenkottil AP, Nkoulou RN, et al. Diagnostic value of ^{13}N-ammonia myocardial perfusion PET: added value of myocardial flow reserve. J Nucl Med. 2012;53:1230−4. https://doi.org/10.2967/jnumed.111.101840.
3. Herzog BA, Husmann L, Valenta I, Gaemperli O, Siegrist PT, Tay FM, et al. Long-term prognostic value of ^{13}N-ammonia myocardial perfusion positron emission tomography added value of coronary flow reserve. J Am Coll Cardiol. 2009;54:150−6. https://doi.org/10.1016/j.jacc.2009.02.069.
4. Patel KK, Spertus JA, Chan PS, Sperry BW, Al Badarin F, Kennedy KF, et al. Myocardial blood flow reserve assessed by positron emission tomography myocardial perfusion imaging identifies patients with a survival benefit from early revascularization. Eur Heart J. 2020;41:759−68. https://doi.org/10.1093/eurheartj/ehz389.
5. Khaing T, Raymond CCW, Chan WX, Hao C, Wong SS. Quantification of myocardial blood flow and myocardial flow reserve with SPECT imaging technique. J Nucl Cardiol. 2019;26:318−23. https://doi.org/10.1007/s12350-017-1152-0.
6. Konerman MC, Lazarus JJ, Weinberg RL, Shah RV, Ghannam M, Hummel SL, et al. Reduced myocardial flow reserve by positron emission tomography predicts cardiovascular events after cardiac transplantation. Circ Heart Fail. 2018;11:e004473. https://doi.org/10.1161/CIRCHEARTFAILURE.117.004473.
7. Spigel ZA, Qureshi AM, Morris SA, Mery CM, Sexson-Tejtel SK, Zea-Vera R, et al. Right ventricle-dependent coronary circulation: location of obstruction is associated with survival. Ann Thorac Surg. 2020;109:1480−7. https://doi.org/10.1016/j.athoracsur.2019.08.066.
8. Sevimli S, Gundogdu F, Aksakal E, Arslan S, Tas H, Islamoglu Y, et al. Right ventricular strain and strain rate properties in patients with right ventricular myocardial infarction. Echocardiography. 2007;24:732−8. https://doi.org/10.1111/j.1540-8175.2007.00470.x.
9. Mazur ES, Mazur VV, Rabinovich RM, Myasnikov KS. Right ventricular longitudinal strain in acute

pulmonary embolism and right ventricular myocardial infarction in patients with McConnell's sign. Kardiologiia. 2020;60:20−7. https://doi.org/10.18087/cardio.2020.7.n1151.

10. Chang WT, Tsai WC, Liu YW, Lee CH, Liu PY, Chen JY, et al. Changes in right ventricular free wall strain in patients with coronary artery disease involving the right coronary artery. J Am Soc Echocardiogr. 2014;27:230−8. https://doi.org/10.1016/j.echo.2013.11.010.
11. Risum N, Valeur N, Søgaard P, Hassager C, Køber L, Ersbøll M. Right ventricular function assessed by 2D strain analysis predicts ventricular arrhythmias and sudden cardiac death in patients after acute myocardial infarction. Eur Heart J Cardiovasc Imaging. 2018;19:800−7. https://doi.org/10.1093/ehjci/jex184.
12. Ivey-Miranda JB, Almeida-Gutiérrez E, Borrayo-Sánchez G, Antezana-Castro J, Contreras-Rodríguez A, Posada-Martínez EL, et al. Right ventricular longitudinal strain predicts acute kidney injury and short-term prognosis in patients with right ventricular myocardial infarction. Int J Cardiovasc Imaging. 2019;35:107−16. https://doi.org/10.1007/s10554-018-1447-5.
13. Nakao R, Nagao M, Yamamoto A, Fukushima K, Watanabe E, Sakai S, et al. Papillary muscle ischemia on high-resolution cine imaging of nitrogen-13 ammonia positron emission tomography: Association with myocardial flow reserve and prognosis in coronary artery disease. J Nucl Cardiol. 2020 [Epub ahead of print] https://doi.org/10.1007/s12350-020-02231-z.
14. Dilsizian V, Bacharach SL, Beanlands RS, Bergmann SR, Delbeke D, Dorbala S, et al. ASNC imaging guidelines/SNMMI procedure standard for positron emission tomography (PET) nuclear cardiology procedures. J Nucl Cardiol. 2016;23:1187−226. https://doi.org/10.1007/s12350-016-0522-3.
15. Cerqueira MD, Weissman NJ, Dilsizian V, Jacobs AK, Kaul S, Laskey WK, et al. Standardized myocardial segmentation and nomenclature for tomographic imaging of the heart. A statement for healthcare professionals from the Cardiac Imaging Committee of the Council on Clinical Cardiology of the American Heart Association. J Nucl Cardiol. 2002;9:240−5. https://doi.org/10.1067/mnc.2002.123122.
16. Fang LL, Zhang PY, Wang C, Wang LM, Ma XM, Shi HW, et al. Two-dimensional strain combined with adenosine stress echocardiography assessment of viable myocardium. Heart Vessels. 2011;26:206−13. https://doi.org/10.1007/s00380-010-0068-2.
17. Qu HY, Yao GH, Sun WY, Chen L, Li XN, Zhang PF, et al. Assessment of ischemic myocardium by

strain-rate imaging during adenosine stress echocardiography. Int J Cardiovasc Imaging. 2007;23:725−32. https://doi.org/10.1007/s10554-006-9183-7.

18. Ran H, Zhang PY, Fang LL, Ma XW, Wu WF, Feng WF. Clinic value of two-dimensional speckle tracking combined with adenosine stress echocardiography for assessment of myocardial viability. Echocardiography. 2012;29:688−94. https://doi.org/10.1111/j.1540-8175.2012.01690.x.
19. Pedrizzetti G, Claus P, Kilner PJ, Nagel E. Principles of cardiovascular magnetic resonance feature tracking and echocardiographic speckle tracking for informed clinical use. J Cardiovasc Magn Reson. 2016;18:51. https://doi.org/10.1186/s12968-016-0269-7.
20. Xu L, Pagano JJ, Haykowksy MJ, Ezekowitz JA, Oudit GY, Mikami Y, et al. Layer-specific strain in patients with heart failure using cardiovascular magnetic resonance: not all layers are the same. J Cardiovasc Magn Reson. 2020;22:81. https://doi.org/10.1186/s12968-020-00680-6.
21. Nakatani S. Left ventricular rotation and twist: why should we learn? J Cardiovasc Ultrasound. 2011;19:1−6. https://doi.org/10.4250/jcu.2011.19.1.1.
22. Kowallick JT, Lamata P, Hussain ST, Kutty S, Steinmetz M, Sohns JM, et al. Quantification of left ventricular torsion and diastolic recoil using cardiovascular magnetic resonance myocardial feature tracking. PLoS One. 2014;9:e109164. https://doi.org/10.1371/journal.pone.0109164.
23. Sakuma M, Ishigaki H, Komaki K, Oikawa Y, Katoh A, Nakagawa M, et al. Right ventricular ejection function assessed by cineangiography--Importance of bellows action. Circ J. 2002;66:605−9. https://doi.org/10.1253/circj.66.605.
24. Kovács A, Lakatos B, Tokodi M, Merkely B. Right ventricular mechanical pattern in health and disease: beyond longitudinal shortening. Heart Fail Rev. 2019;24:511−20. https://doi.org/10.1007/s10741-019-09778-1.
25. Kawaguchi N, Okayama H, Kawamura G, Shigematsu T, Takahashi T, Kawada Y, et al. Clinical usefulness of coronary flow reserve ratio for the detection of significant coronary artery disease on ^{13}N-Ammonia positron emission tomography. Circ J. 2018;82:486−93. https://doi:10.1253/circj.CJ-17-0745.
26. Kawakubo M, Yamasaki Y, Kamitani T, Sagiyama K , Matsuura Y, Hino T, et al. Clinical usefulness of right ventricular 3D area strain in the assessment of treatment effects of balloon pulmonary angioplasty in chronic thromboembolic pulmonary hypertension: comparison with 2D feature-tracking MRI. Eur Radiol. 2019;29:4583−92. https://doi.org/10.1007/s00330-019-6008-3.

27. Kawakubo M, Nagao M, Ishizaki U, Shiina Y, Inai K, Yamasaki Y, et al. Feature-tracking MRI fractal analysis of right ventricular remodeling in adults with congenitally corrected transposition of the great arteries. Radiol Cardiothorac Imaging. 2019;1:e190026. https://doi.org/10.1148/ryct.2019190026.

FIGURE LEGENDS

Fig.1 Semi-automatic feature-tracking in cine imaging of positron emission tomography

Images from left to right indicate the flow of the image processing. First, the endocardial border was manually defined as a freehand line at end-diastole (green square). Then, the line was replaced with 7 points, and the template image centered on each point was tracked through a cardiac cycle. The upper row indicates the tracking of the right ventricular free wall on horizontal long-axis images (magenta square). The lower row indicates the tracking of the left ventricular inferior wall on vertical long-axis images (yellow square).

Fig.2 Systolic longitudinal strain values according to myocardial flow reserve status

(a) Right ventricular free-wall longitudinal strain values in patients with RCA-MFR<2.0 (purple/dark purple), with LAD/LCx-MFR<2.0 (blue/dark blue), with regional MFR≥2.0 for all territories (red/dark red), and control (green/dark green). (b) Left ventricular inferior-wall longitudinal strain values in patients with RCA-MFR<2.0 (purple/dark purple), with LAD/LCx-MFR<2.0 (blue/dark blue), with regional MFR≥2.0 for all territories (red/dark red), and control (green/dark green).

**P<0.01, *P<0.05. RV, right ventricular; LV, left ventricular; MFR, myocardial flow reserve; RCA, right coronary artery; LAD, left anterior descending artery; LCx, left circumflex coronary artery.

Fig.3 Systolic longitudinal strain values according to the presence of ischemic image findings

Right ventricular free-wall longitudinal strain values in patients with RCA ischemia (purple/dark purple), with LAD/LCx ischemia (blue/dark blue), without ischemia (red/dark red), and control (green/dark green).

**P<0.01, *P<0.05. RV, right ventricular; RCA, right coronary artery; LAD, left anterior descending artery; LCx, left circumflex coronary artery

Fig.4 ^{13}N-ammonia PET images (left) and the RV-LS curve (right) for a woman in her 50s with RCA-MFR=1.20 (blue) and for a man in his late 60s with RCA-MFR≥3.0 (red)

In the patients with RCA-MFR=1.20, stressed RV-LS (blue solid curve) was reduced compared to the resting state (blue dashed line). In patients with RCA-MFR≥3.0, stressed RV-LS (red solid curve) increased compared to that in the resting state (red dashed line).

PET, positron emission tomography; RV-LS, right ventricular longitudinal strain; RCA, right coronary artery; MFR, myocardial flow reserve.

Fig.5 Correlations between right ventricular free-wall strains and regional myocardial flow reserves

Scatter plots show the correlations between longitudinal strain and regional myocardial flow reserve. Plots in the upper and lower rows indicate the values in the stressed and resting states, respectively.

r_S, Spearman's correlation coefficient; *r*, Pearson's correlation coefficient; RV, right ventricular; MFR, myocardial flow reserve; RCA, right coronary artery; LAD, left anterior descending artery; LCx, left circumflex coronary artery.

Fig.6 Correlations between left ventricular inferior-wall strains and regional myocardial flow reserves.

Scatter plots show the correlations between longitudinal strain and regional myocardial flow reserve. Plots in the upper and lower rows indicate the values in the stressed and resting states, respectively.

r_S, Spearman's correlation coefficient; *r*, Pearson's correlation coefficient; LV, left ventricular; MFR, myocardial flow reserve; RCA, right coronary artery; LAD, left anterior descending artery; LCx, left circumflex coronary artery.

Figure

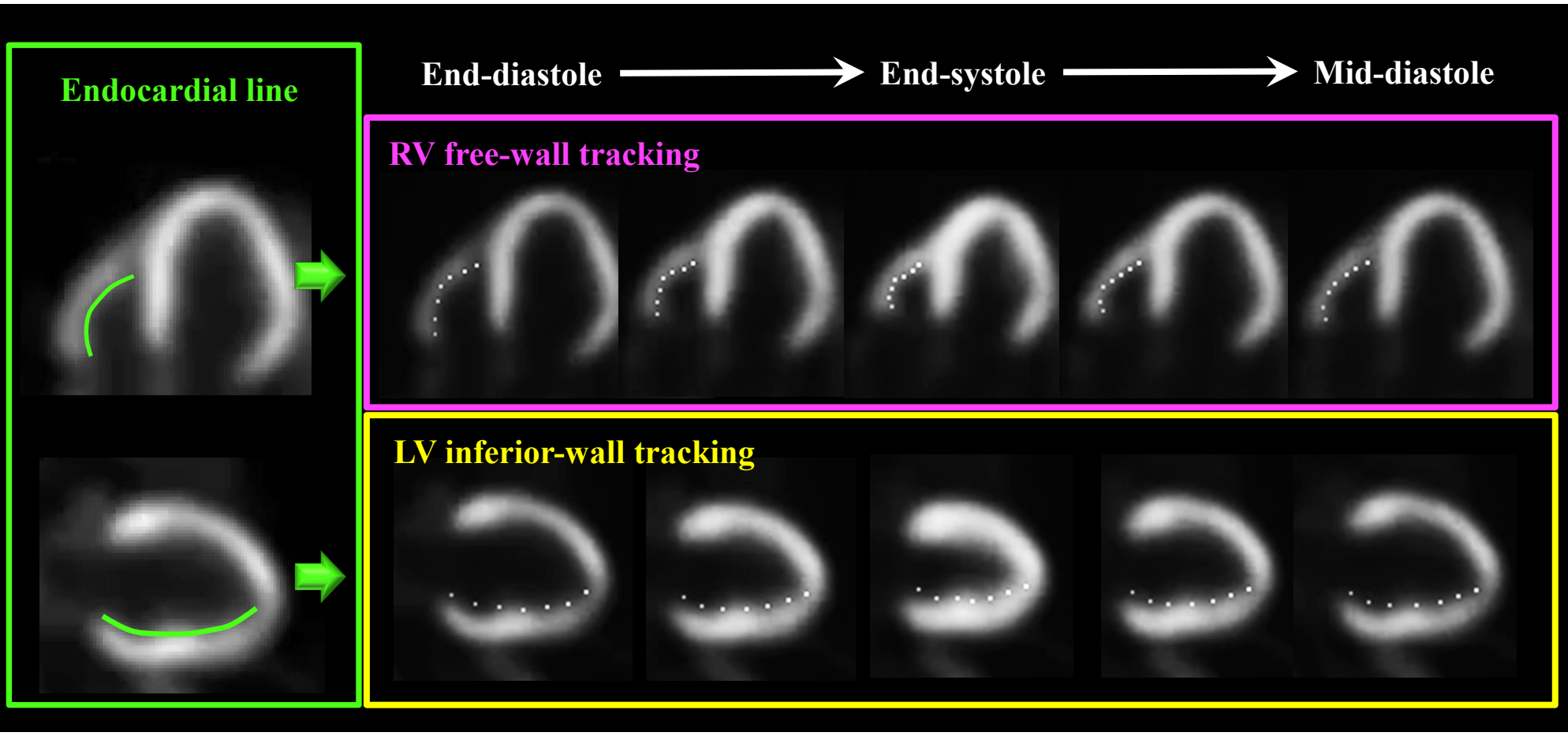

FIGURE 1. Semi-automatic feature-tracking in cine imaging of positron emission tomography.

Images from left to right indicate the flow of the image processing. First, the endocardial border was manually defined as a freehand line at end-diastole (green square). Then, the line was replaced with 7 points, and the template image centered on each point was tracked through a cardiac cycle. The upper row indicates the tracking of the right ventricular free wall on horizontal long-axis images (magenta square). The lower row indicates the tracking of the left ventricular inferior wall on vertical long-axis images (yellow square).

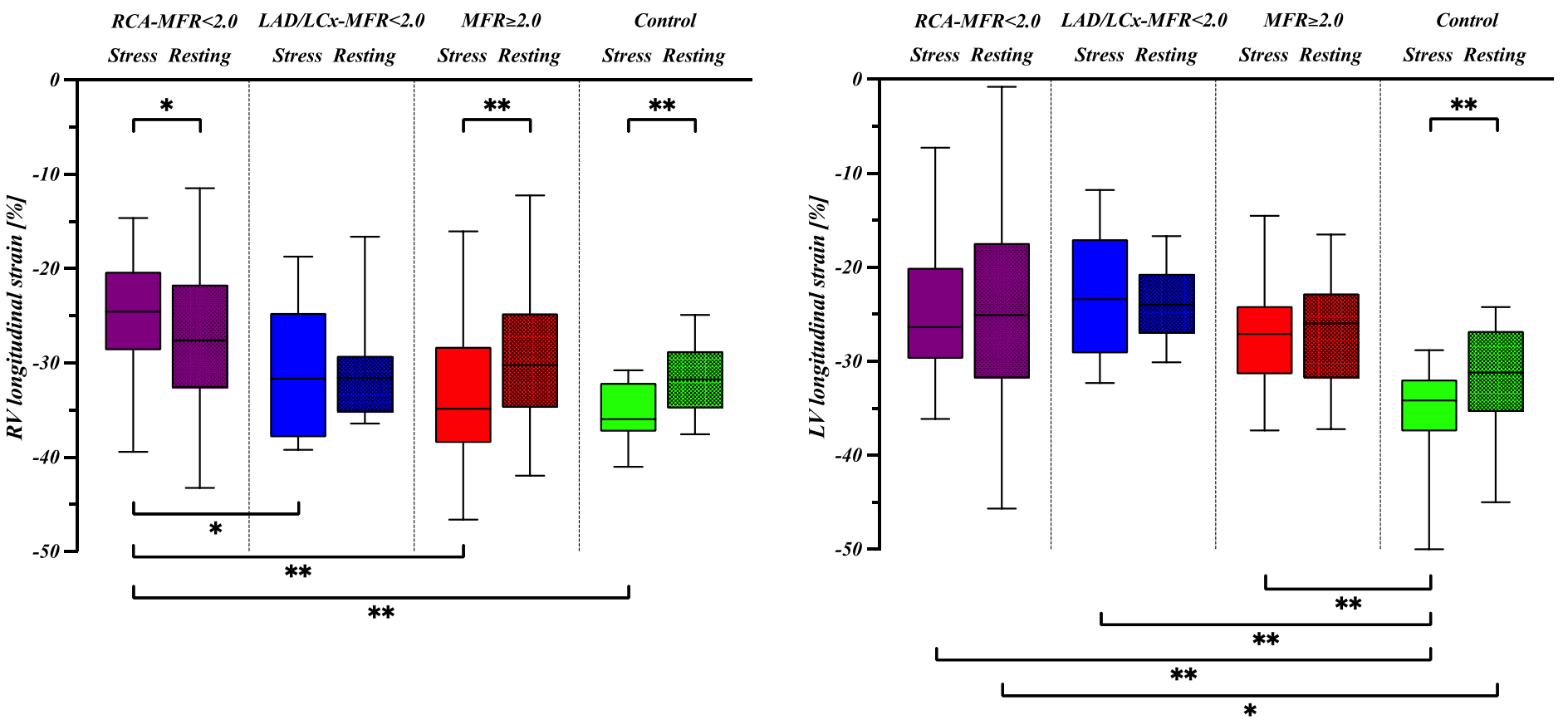

FIGURE 2. Systolic longitudinal strain values according to myocardial flow reserve status.

(a) Right ventricular free-wall longitudinal strain values in patients with RCA-MFR<2.0 (purple/dark purple), with LAD/LCx-MFR<2.0 (blue/dark blue), with regional MFR≥2.0 for all territories (red/dark red), and control (green/dark green). (b) Left ventricular inferior-wall longitudinal strain values in patients with RCA-MFR<2.0 (purple/dark purple), with LAD/LCx-MFR<2.0 (blue/dark blue), with regional MFR≥2.0 for all territories (red/dark red), and control (green/dark green).

**P<0.01, *P<0.05. RV, right ventricular; LV, left ventricular; MFR, myocardial flow reserve; RCA, right coronary artery; LAD, left anterior descending artery; LCx, left circumflex coronary artery.

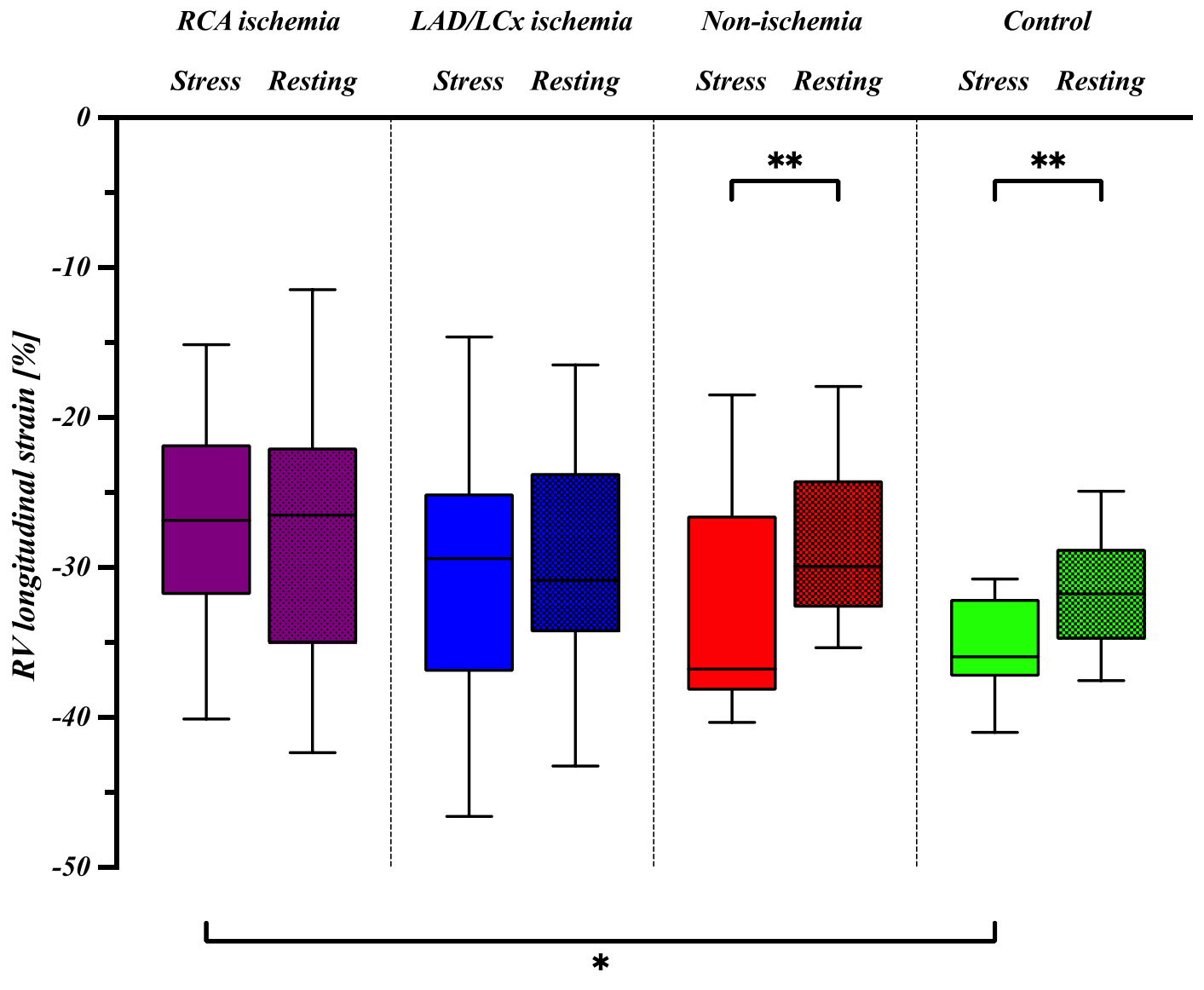

FIGURE 3. Systolic longitudinal strain values according to presence of ischemic image findings.

Right ventricular free-wall longitudinal strain values in patients with RCA ischemia (purple/dark purple), with LAD/LCx-ischemia (blue/dark blue), without ischemia (red/dark red), and control (green/dark green).
**P<0.01, *P<0.05. RV, right ventricular; RCA, right coronary artery; LAD, left anterior descending artery; LCx, left circumflex coronary artery.

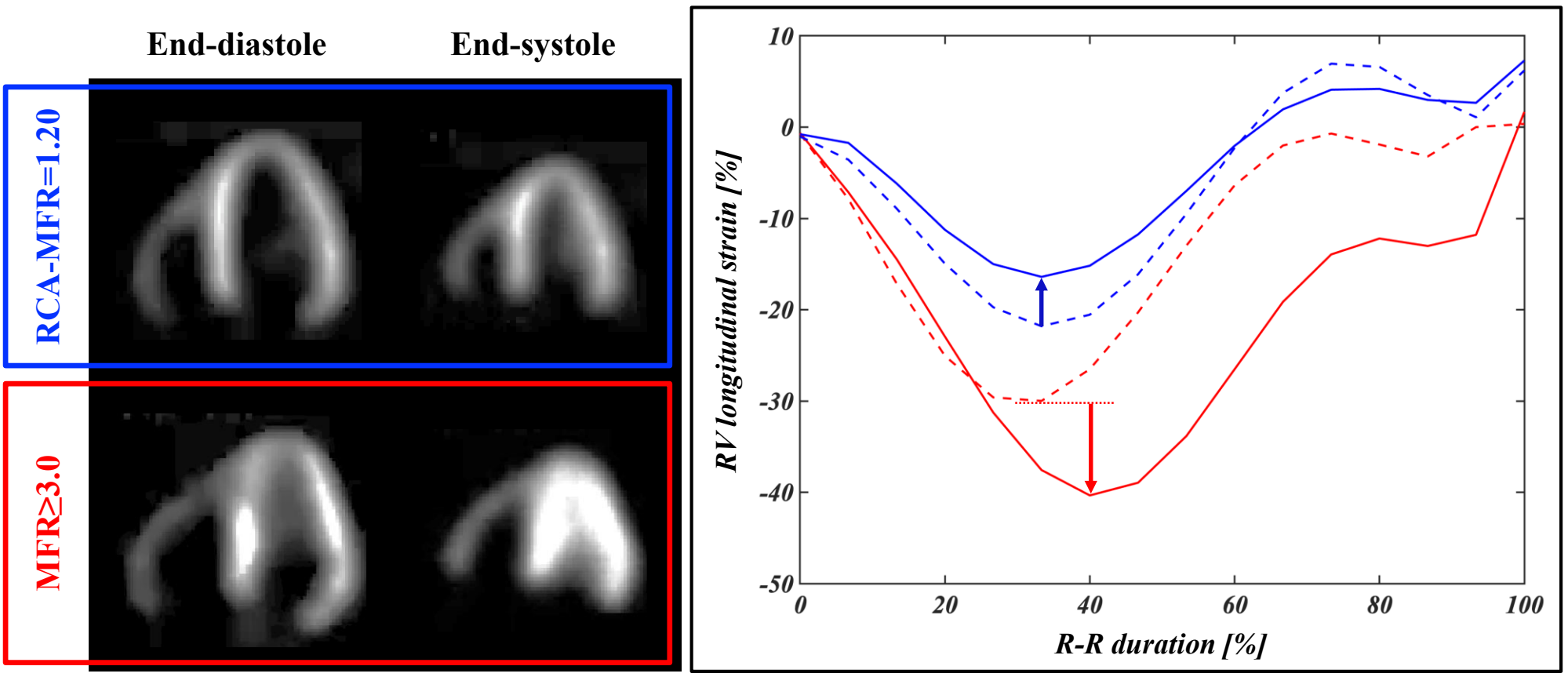

FIGURE 4. 13N-ammonia PET images (left) and the RV-LS curve (right) for a woman in her 50s with RCA-MFR=1.20 (blue) and for a man in his late 60s with RCA-MFR≥3.0 (red)

In the patients with RCA-MFR=1.20, stressed RV-LS (blue solid curve) was reduced compared to the resting state (blue dashed line). In patients with RCA-MFR≥3.0, stressed RV-LS (red solid curve) increased compared to that in the resting state (red dashed line).

PET, positron emission tomography; RV-LS, right ventricular longitudinal strain; RCA, right coronary artery; MFR, myocardial flow reserve.

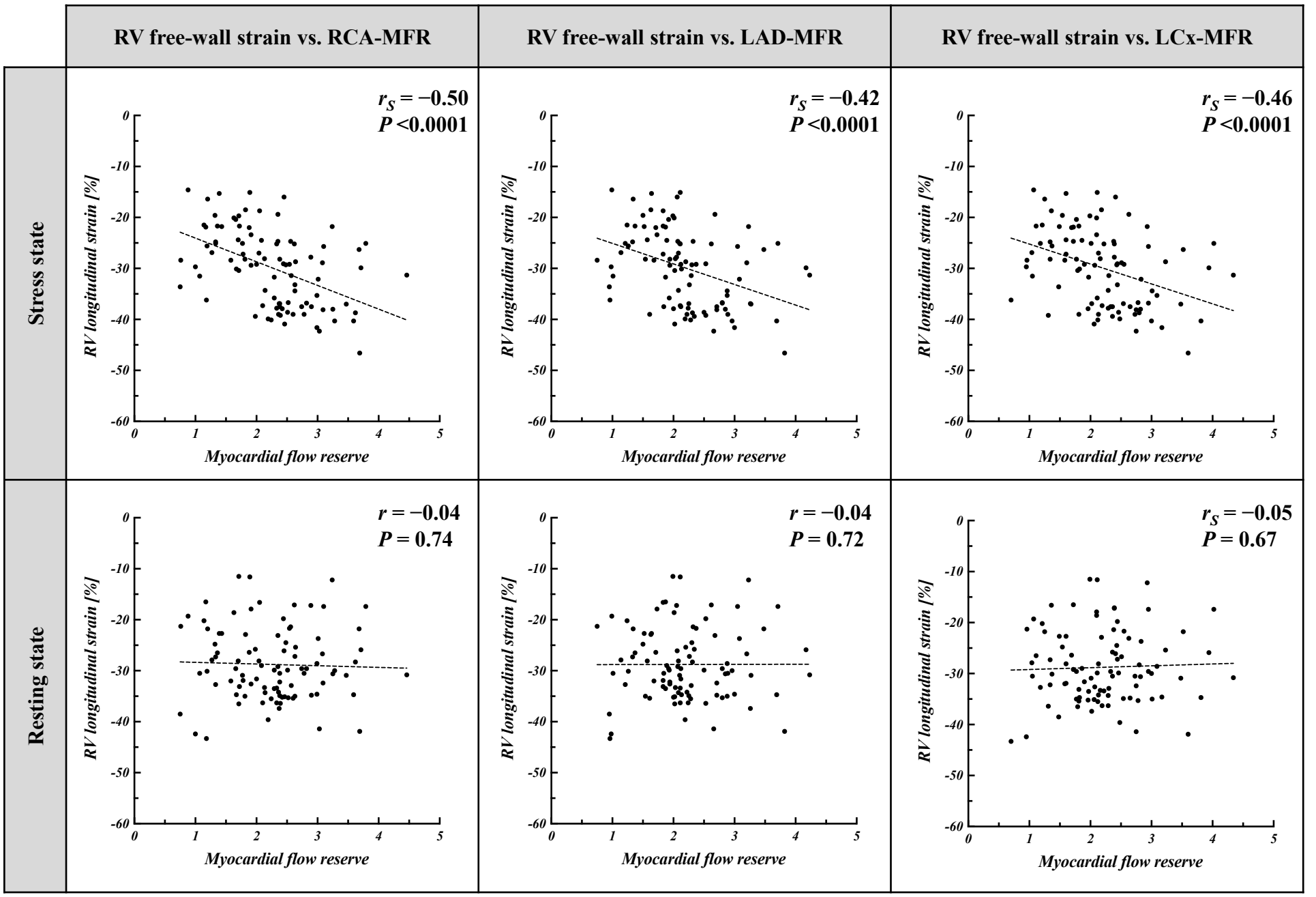

FIGURE 5. Correlations between right ventricular free-wall strains andregional myocardial flow reserves.

Scatter plots show the correlations between longitudinal strain and regional myocardial flow reserve. Plots in the upper and lower rows indicate the values in the stressed and resting states, respectively.
rS, Spearman's correlation coefficient; r, Pearson's correlation coefficient; RV, right ventricular; MFR, myocardial flow reserve; RCA, right coronary artery; LAD, left anterior descending artery; LCx, left circumflex coronary artery.

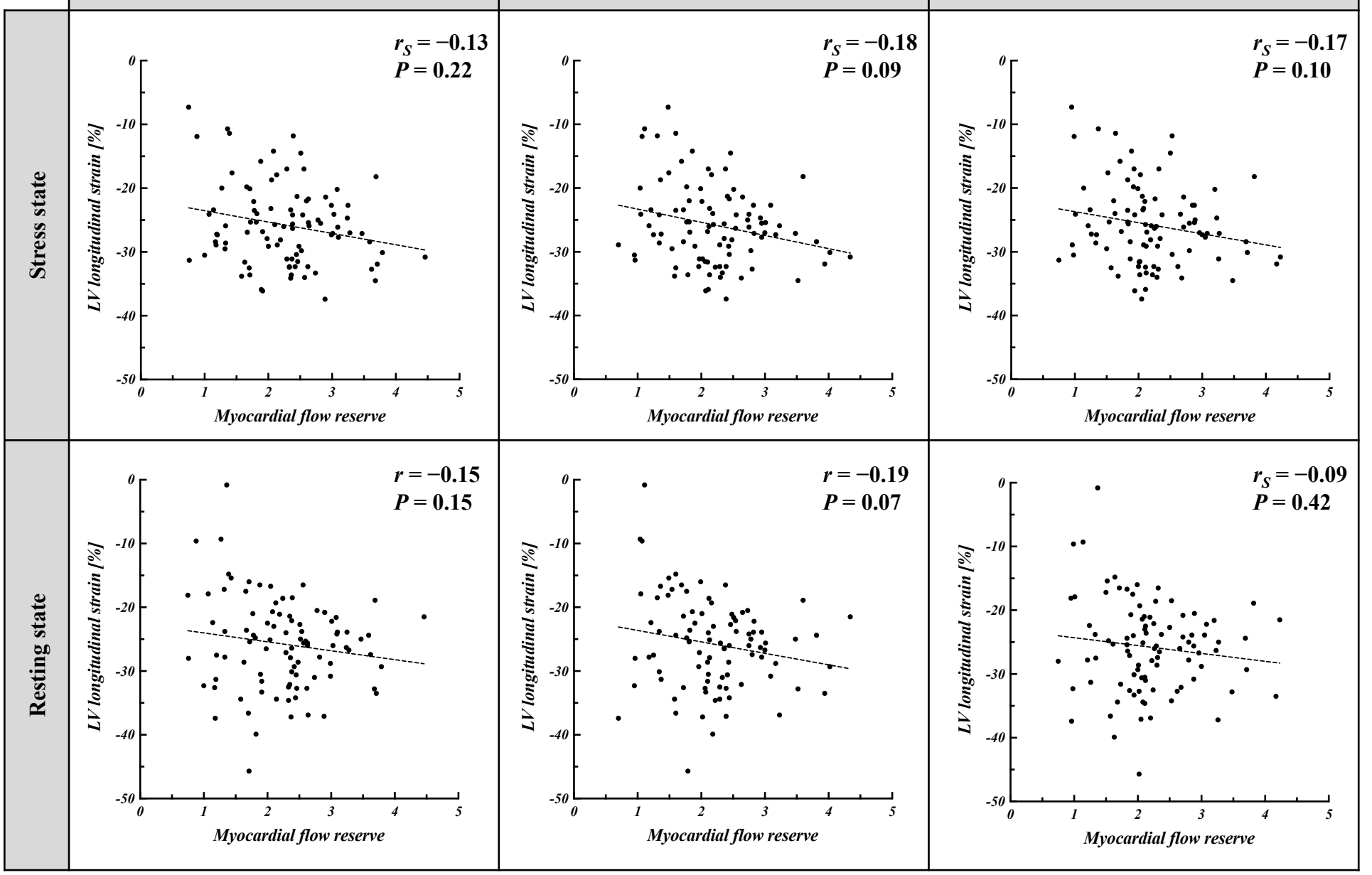

FIGURE 6. Correlations between left ventricular inferior-wall strains and regional myocardial flow reserves.

Scatter plots show the correlations between longitudinal strain and regional myocardial flow reserve. Plots in the upper and lower rows indicate the values in the stressed and resting states, respectively.
rS, Spearman's correlation coefficient; r, Pearson's correlation coefficient; LV, left ventricular; MFR, myocardial flow reserve; RCA, right coronary artery; LAD, left anterior descending artery; LCx, left circumflex coronary artery.

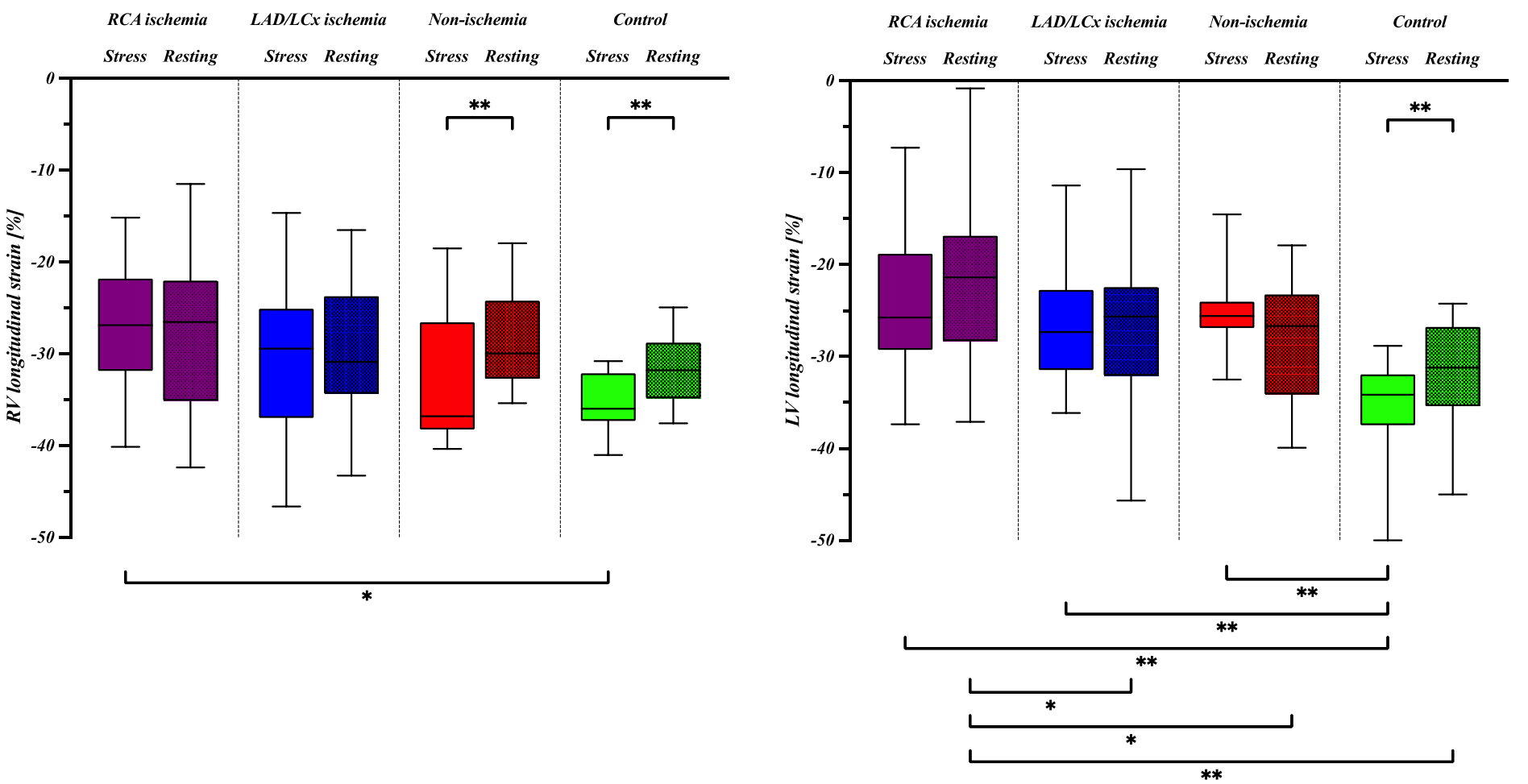

FIGURE 3. Systolic longitudinal strain values according to presence of ischemic image findings.

(a) Right ventricular free-wall longitudinal strain values in patients with RCA ischemia (purple/dark purple), with LAD/LCx-ischemia (blue/dark blue), without ischemia (red/dark red), and control (green/dark green). (b) Left ventricular inferior-wall longitudinal strain values in patients with RCA ischemia (purple/dark purple), with LAD/LCx-MFR ischemia (blue/dark blue), without ischemia (red/dark red), and control (green/dark green).

**P<0.01, *P<0.05. RV, right ventricular; LV, left ventricular; RCA, right coronary artery; LAD, left anterior descending artery; LCx, left circumflex coronary artery.

TABLE 1 Baseline patient characteristics and ^{13}N-ammonia PET measurements

Characteristics	RCA-MFR<2.0	LAD-MFR<2.0 or LCx-MFR<2.0	MFR≥2.0	Control
Number	34	11	48	10
Age [year]	69 ± 11	68 ± 11	67 ± 10	41 ± 15
Male/Female	20/14	7/4	34/14	6/4
Cardiovascular risk factor				
Hypertension	24	7	36	0
Dyslipidemia	15	5	23	0
Diabetes mellitus	20	9	38	0
Smoking	15	6	22	0
Positive family history	5	4	13	0
Clinical history of CAD				
History of myocardial infarction	8	2	5	0
Previous PCI	8	4	9	0
Previous CABG	3	1	4	0
Ammonia PET measurements				
SSS	9 ± 9	8 ± 8	2 ± 3	2 ± 3
SRS	3 ± 4	3 ± 4	1 ± 1	1 ± 1
SDS	6 ± 8	5 ± 5	2 ± 3	1 ± 2
Stress MBF [mL/g/min]	1.60 ± 0.56	1.98 ± 0.40	2.43 ± 0.54	2.43 ± 1.00
Resting MBF [mL/g/min]	1.05 ± 0.29	1.00 ± 0.21	0.92 ± 0.22	1.06 ± 0.28
Global-MFR	1.5 ± 0.4	2.0 ± 0.1	2.7 ± 0.6	2.2 ± 0.6
RCA-MFR	1.5 ± 0.4	2.3 ± 0.2	2.8 ± 0.5	2.3 ± 0.6
LAD-MFR	1.6 ± 0.4	2.0 ± 0.2	2.7 ± 0.6	2.3 ± 0.6
LCx-MFR	1.6 ± 0.4	1.8 ± 0.3	2.7 ± 0.6	2.2 ± 0.6
Stress LVEDV [mL]	105 ± 33	101 ± 27	99 ± 25	76 ± 15

Stress LVESV [mL	44 ± 29	38 ± 20	30± 16	17 ± 5
Stress LVEF [%]	62 ± 16	64 ± 12	71 ± 9	78 ± 4
Resting LVEDV [mL]	92 ± 35	89 ± 28	85 ± 23	71 ± 15
Resting LVESV [mL]	38 ± 29	31 ± 20	25 ± 13	17 ± 5
Resting LVEF [%]	66 ± 15	67 ± 14	72 ± 9	76 ± 5

Unless otherwise indicated, data are presented as the mean ± standard deviation. CAD, coronary artery disease; PCI, percutaneous coronary intervention; CABG, coronary artery bypass grafting; PET, positron emission tomography; SSS, summed stress score; SRS, summed rest score; SDS, summed difference score; MBF, myocardial blood flow; MFR, myocardial flow reserve; RCA, right coronary artery; LV, left ventricular; EDV, end-diastolic volume; ESV, end-systole volume; EF, ejection fraction.

TABLE 2 Reproducibility of longitudinal strain analyses

	Intra-observer reproducibility			Inter-observer reproducibility		
Parameter	Bias (LOA)	SDD	ICC (95% CI)	Bias (LOA)	SDD	ICC (95% CI)
Stress RV-LS	−1.40 (−16.8 to 14.1)	7.9	0.85 (0.83 to 0.87)	−1.0 (−18.3 to 16.3)	8.8	0.82 (0.80 to 0.87)
Resting RV-LS	−0.3 (−14.0 to 13.4)	7.0	0.88 (0.85 to 0.90)	−0.03(−16.1 to 16.1)	8.2	0.83 (0.80 to 0.86)
Stress LV-LS	0.8 (−4.0 to 5.5)	2.4	0.97 (0.83 to 0.99)	−0.29 (−4.97 to 4.39)	2.5	0.97 (0.96 to 0.97)
Resting LV-LS	−0.46 (−4.4 to 3.5)	2.0	0.98 (0.97 to 0.98)	−0.15 (−4.24 to 3.94)	2.1	0.97 (0.97 to 0.98)

RV, right ventricular; LV, left ventricular; LS, longitudinal strain; LOA, limit of agreement; SDD, standard deviation of the difference; ICC, intraclass correlation coefficient; CI, confidence interval.